Journal of Electrochemistry

Volume 28
Issue 2 *Special Issue: Frontier of Electrochemistry (I)*

2022-02-28

Facet Dependent Oxygen Evolution Activity of Spinel Cobalt Oxides

Li-Hua Zhang

Hong-Yuan Chuai
1. Key Laboratory for Green Chemical Technology of Ministry of Education, School of Chemical Engineering and Technology, Tianjin University, Tianjin 300072, China;, chuaihongyuan@tju.edu.cn

Hai Liu

Qun Fan

Si-Yu Kuang

Sheng Zhang
1. Key Laboratory for Green Chemical Technology of Ministry of Education, School of Chemical Engineering and Technology, Tianjin University, Tianjin 300072, China;3. Zhejiang Institute of Tianjin University, Ningbo 315201, Zhejiang, China;, sheng.zhang@tju.edu.cn

Xin-Bin Ma

Recommended Citation

Li-Hua Zhang, Hong-Yuan Chuai, Hai Liu, Qun Fan, Si-Yu Kuang, Sheng Zhang, Xin-Bin Ma. Facet Dependent Oxygen Evolution Activity of Spinel Cobalt Oxides[J]. *Journal of Electrochemistry*, 2022 , 28(2): 2108481.
DOI: 10.13208/j.electrochem.210848
Available at: https://jelectrochem.xmu.edu.cn/journal/vol28/iss2/3

电 化 学
J. Electrochem. 2022, 28(2), 2108481 (1 of 11)

【Article】 **DOI**: 10.13208/j.electrochem.210848 **Http**://electrochem.xmu.edu.cn

Facet Dependent Oxygen Evolution Activity of Spinel Cobalt Oxides

Li-Hua Zhang[1,2], Hong-Yuan Chuai[1*], Hai Liu[1], Qun Fan[1], Si-Yu Kuang[1], Sheng Zhang[1,3*], Xin-Bin Ma[1,3]

(*1. Key Laboratory for Green Chemical Technology of Ministry of Education, School of Chemical Engineering and Technology, Tianjin University, Tianjin 300072, China; 2. Petrochemical Catalyst Lab., Lanzhou Petrochemical Research Center, Petrochemical Research Institute, PetroChina Company Limited, Lanzhou 730060, China; 3. Zhejiang Institute of Tianjin University, Ningbo 315201, Zhejiang, China*)

Abstract: Water splitting is a promising technology to produce clean hydrogen if powered by renewable energies, where oxygen evolution is the rate determining step at an anode. Here we adjust the different crystal planes of the cobalt oxides catalyst to expose more effective active sites through a hydrothermal process, so as to improve the reaction activity for oxygen evolution. The samples were well characterized by TEM, SEM and XRD. Among the three synthetic crystal planes (100), (111) and (110) of spinel cobalt oxides, the (100) crystal plane has the highest intrinsic activity. Combining *in-situ* infrared and DFT calculations, we observed that the oxygen evolution reaction reached the lowest energy barrier on the (100) plane of the cobalt oxide crystal. Further XPS analysis showed that the highest Co^{3+}/Co^{2+} ratio was observed on the surface of the nanocube samples, indicating that Co^{3+} is a more active site for oxygen evolution catalytic activity.

Key words: water splitting; oxygen evolution; spinel cobalt oxide; facet dependent; nanocubes

1 Introduction

Today, with advanced technology in the 21st century, environmental pollution and energy crisis have become the most concerned issues. Producing hydrogen by splitting water from clean electrical energy, which is generated by renewable energy such as solar energy and wind energy, is an important way to realize green hydrogen energy[1]. The water-splitting device consists of the cathodic hydrogen evolution reaction (HER) and the anodic oxygen evolution reaction (OER)[2-4]. Since there are four protons transferred during the whole process, OER is a slow dynamic reaction with a high reaction energy barrier[5]. In addition, OER could be also coupled with CO_2 reduction reaction in CO_2 electrolyzers[6-7]. Till now, developing highly efficient electrocatalysts for the sluggish OER remains a crucial bottle-neck on the way to the applications of water splitting for producing clean fuel[8-10].

IrO_2 and RuO_2 are reported as highly active catalysts for OER, however, their large-scale applications are unrealizable due to the scarcity of resources and high price[11]. Therefore, developing highly efficient and cheap catalysts based on earth-abundant non-noble metals for OER is paramount and urgent. Compared with noble metal oxides, a general transition metal oxide, Co_3O_4, has been extensively investigated due to its low cost, high catalytic activity and easy availability[12]. However, the catalytic property of Co_3O_4

Cite as: Zhang L H, Chuai H Y, Liu H, Fan Q, Kuang S Y, Zhang S, Ma X B. Facet dependent oxygen evolution activity of spinel cobalt oxides. *J. Electrochem.*, 2022, 28(2): 2108481.

Received: 2021-10-25; Revised: 2021-11-30. * Hong-Yuan Chuai, Tel: (86)18920501321, E-mail: chuaihongyuan@tju.edu.cn, Sheng Zhang, Tel: (86)13116156703, E-mail: sheng.zhang@tju.edu.cn

is not satisfactory, in order to further improve its catalytic activity and durability, a series of methods such as the use of synergistic effects[13], increasing defect sites[14], doping effects[15], and increasing specific surface area[16], have been explored to reduce the reaction energy barrier and improve the reaction activity.

Among these, crystal regulation of Co_3O_4 is an effective way to enhance the catalytic activity for OER. In recent years, many researchers have studied the relationship between the crystal planes of Co_3O_4 and the performance of OER. Zhang et al. reported that Co_3O_4 nanorods with the dominantly exposed planes of (110) were more active to OER catalysis than those with (100)[17]; Liu et al. found that Co_3O_4 crystals exposed with (111) facets showed the highest OER and HER activities[18]; Sun et al. synthesized Co_3O_4 nanocubes, nanosheets, and nanoplates with different exposed planes of (100), (110), and (111), and demonstrated that different electrocatalytic performances were possibly attributed to the abundance ratios of Co^{3+}/Co^{2+} over the different exposed planes[19]. Since there are controversial results between high-performance facet and its OER performance, we designed experiment to clarify the relationship between the facet and OER performance from the perspective view of theory and experiment.

The monitoring of reaction intermediates through a variety of spectroscopic characterization has a positive effect on understanding the structure-activity relationship of catalysts and designing efficient catalysts[20]. In this work, we constructed the spinel cobalt oxide catalysts with different morphologies that expose different crystal faces and probed the active sites during the reaction process in order to systematically investigate the effect of crystal plane on the OER performance of Co_3O_4. Combined with *in-situ* characterization technology and density functional theory (DFT) calculation, the active sites of spinel cobalt oxide in the OER reaction were explored in detail. *In-situ* FT-IR spectra captured the peaks of O_2 and OOH* intermediate generated in the OER process over cobalt oxide nanocubes with the (100) facet, while the DFT calculations confirmed that the (100) facet had the lowest energy barrier for OER. This work laid the foundation for a deep understanding of the structure-activity relationship between the cobalt oxide catalyst and the OER reaction activity, thereby providing a reliable idea for the design of high-efficiency catalysts in the future.

2 Experimental

2.1 Catalyst Synthesis

Cobalt oxide nanoparticles with various morphologies were synthesized by a hydrothermal method with or without dispersant according to the previous report[21].

Irregular cobalt oxide particles took 11.6 g of cobalt nitrate hexahydrate and 0.4 g of sodium hydroxide, and dissolved in 40 mL of deionized water briefly. The sodium hydroxide alkali solution was added dropwise to the cobalt nitrate solution while stirring. After aged for 30 min at room temperature, a blue-green suspension was formed. The suspension was transferred to a Teflon-lined autoclave and heated at 180 ℃ for 5 h. Naturally cool to room temperature, and then centrifuge to obtain the precipitate. It was washed for three times with deionized water and ethanol, and then dried at 60 ℃ for 12 h. The product was calcined at 500 ℃ for 3 h with a heating rate of 2 $^{\circ}C \cdot min^{-1}$ to obtain the black solid powder.

Cubic cobalt oxide particles were obtained with 23.3 g cobalt nitrate hexahydrate and 0.4 g sodium hydroxide by the same method as depicted above.

Flake cobalt oxide particles needed to add a dispersant to participate in the synthesis. 1.3 g of anhydrous cobalt chloride solids and 5.6 g of polyvinylpyrrolidone were dissolved in 30 mL of deionized water and stirred thoroughly to form the red transparent solution 1, while 1.1 g of potassium hydroxide was dissolved in 20 mL of deionized water to form the solution 2. The solution 2 was added to the solution 1 drop by drop and aged for 30 min. The mixed solution reacted for 12 h in a reducing atmosphere. The product was centrifuged and washed with deionized water and ethanol, and then dried at 60 ℃ for 12 h. Followed by calcining at 300 ℃ for 2 h with a heating rate of 2 $^{\circ}C \cdot min^{-1}$, the flake cobalt oxide particles

were obtained.

Three morphologies of cobalt oxide nanoparticles are named as Nanoparticles, Nanocubes and Plate-like sheets.

2.2 Physical Characterization

X-ray diffraction (XRD, D8-Focus X-ray diffractometer manufactured by Bruker AXS Co., Ltd., Germany) was used to identify the crystal structure and local crystallinity of Co_3O_4 nanocrystals. Scanning electron microscopy (SEM, Regulus 8100 equipped with energy spectrometer) was used to investigate the morphology of Co_3O_4 nanocrystals. Transmission electron microscopy (TEM, JEM-2100F Field Emission Transmission Electron Microscope from JEOL) was used to investigate the microstructure of Co_3O_4 and obtain electron diffraction patterns. The surface elemental composition was characterized by X-ray photoelectron spectroscopy (XPS, K-Alpha+, manufactured by ThermoFisher Scientific Company) using a pass energy of 20 eV and an Al K_α X-ray source operated at 200 W.

2.3 Electrochemical Characterization

Electrochemical evaluation was performed using rotating disc electrode (RDE) voltammetry. The Co_3O_4 nanocrystals were dispersed in isopropanol containing 0.2wt% of Nafion solution (LIQUIONs LQ-1115), forming 2 mg·mL^{-1} electrode preparation solution. After sonication, the working electrode was prepared by depositing the catalyst solution onto a glassy carbon electrode (PINE Research Instrument) to achieve catalyst loadings of approximately 0.25 mg·cm^{-2}.

Operando attenuated total reflection-Fourier-transform infrared (Thermo Scientific Nicolet iS50 FTIR Spectrometer at a spectral resolution of 4 cm^{-1}, equipped with situ reaction cell) was used to monitor the intermediates generated in the reaction. Au film was deposited on the basal plane of a hemicylindrical Si prism by ion sputtering and then, the desired amount of catalyst ink was pipetted and loaded on the Au film. After drying, the catalyst layer was immersed in 1 mol·L^{-1} KOH electrolyte and worked as the working electrode. The Pt wire and Hg/HgO were used as the counter electrode and reference electrode, respectively. FT-IR spectra were recorded after 60 s electrolysis at different potentials supplied by CHI 1242 electrochemical workstation.

2.4 DFT Calculation

All the calculations were performed within the framework of the density functional theory (DFT) as implemented in the Vienna Ab initio Software Package (VASP 5.3.5) code within the PerdewBurke-Ernzerhof (PBE) generalized gradient approximation and the projected augmented wave (PAW) method. The cutoff energy for the plane-wave basis set was set to 400 eV. The Brillouin zone of the surface unit cell was sampled by Monkhorst-Pack (MP) grids, with a k-point mesh for Co_3O_4 structure optimizations. The Co_3O_4(111) surface was determined by 3×3×1 Monkhorst-Pack grid. The convergence criterion for the electronic self-consistent iteration and force was set to 10^{-5} eV and 0.01 eV·Å^{-1}, respectively. A 3×3 supercell of the Co_3O_4(111) surface including 3 layers was constructed to model the Co_3O_4 catalyst in this work. The PBE+U approach was applied to calculations of the electronic structure of Co_3O_4 which can partly reduce the underestimation of the electronic band gap and the excessive tendency to delocalize the electron density. In this work, we set the Hubbard parameter to U-J = 3 eV for Co, which ensures a good qualitative description of structure and electronic properties of Co oxide. A vacuum layer of 15 Å was introduced to avoid interactions between periodic images.

3 Results and Discussion

The morphology, average particle size and exposed crystal plane of each cobalt oxide material were characterized in detail by SEM and TEM. As shown in Figure 1(A) and (B), the edges of nanoparticles were uneven and the particle size was about 20 ~ 50 nm. The surface HRTEM image obtained from nanoparticles in Figure 1(C) obviously shows that the lattice fringe corresponding to the (111) planes is 0.419 nm. As shown in Figure 1(D) and (E), the cobalt oxide was well constructed into nanocubes with approximately 500 nm in size. The lattice fringe and the inter-planar angle could be confirmed by analysis of HRTEM, it could be clearly demonstrated that the

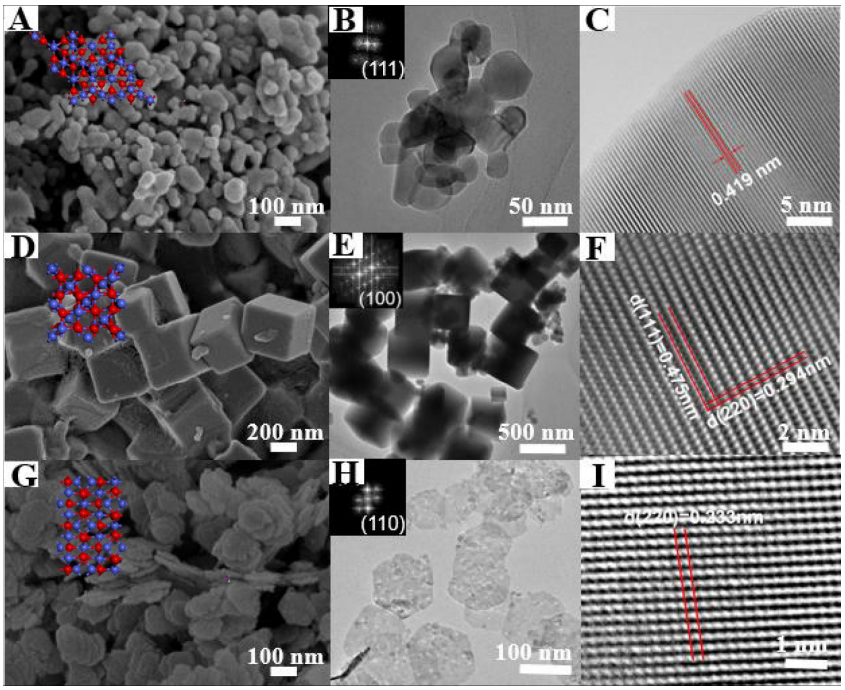

Figure 1. SEM (left), TEM (middle) and HRTEM (right) images of Nanoparticles (A, B and C); Nanocubes (D, E and F); Plate-like sheets (G, H and I); the inset figures in (A), (D), and (G) are the constructed models of different facets. (color on line)

cubic cobalt oxide consisted of six(100) closed facets (Figure 1(F)). For the plate-like sheets, as shown in Figure 1(G) and (H), it had clear edges, with a side length of about 100 nm and 110° between the adjacent sides, presenting a hexagonal shape. The diffraction spot of plate-like cobalt oxides with a lattice spacing of 0.233 nm corresponded to the value of the (110) plane (Figure 1(I)).

Cobalt oxide nanocrystals with different exposed faces were then characterized by XRD diffraction patterns. As shown in Figure 2, for the cobalt oxide samples with different morphologies, the diffraction peaks could identify to be spinel Co_3O_4(JCPDS card number 65-3103). The cobalt oxide particles exhibited an X-ray diffraction (XRD) with the prominent peaks at 19.0°, 31.3°, 36.9°, 38.5°, 44.8°, 59.4°, and 65.2°, which can be assigned to the planes of (111), (220), (311), (222), (400), (511), and (440), respectively.

The oxidation state of cobalt in different samples was investigated by X-ray photoelectron spectroscopy (XPS). The regional Co 2p spectra of each sample are shown in Figure 3. The two main peaks located near 780.0 and 795 eV can be attributed to Co $2p_{3/2}$ and Co $2p_{1/2}$ orbitals, which indicates that both Co^{2+} and Co^{3+} species exist in all cobalt oxide samples[22, 23]. In order to further analyze the valence state distribution of Co element, the Co $2p_{3/2}$ orbital was deconvoluted and integrated into two subpeaks of 779.8 eV and 781.7 eV, which are attributed to the trivalent cobalt ion (Co^{3+}) and the divalent cobalt ion (Co^{2+}), respectively (Figure 3(B)), and the corresponding satellite peaks could be observed at 789.3 eV and 785.4 eV[24, 25]. Ac-

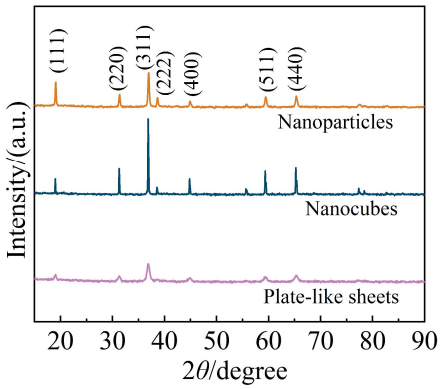

Figure 2. XRD patterns of cobalt oxides with different shapes (color on line)

cording to the peak area ratio of the two subpeaks, the content ratio of trivalent cobalt and divalent cobalt (Co^{3+}/Co^{2+}) in the surface atoms can be estimated semi-quantitatively. The results are shown in Table 1 where the molar ratio of Co^{3+}/Co^{2+} was extracted from fitting parameters. As seen from Table 1, the molar ratio of Co^{3+}/Co^{2+} corresponding to Nanocubes was 2.29, which is higher than those of the other two. According to the literature, the higher valence state cobalt is the main active sites for OER[17, 19]. Therefore, the nanocubes sample is expected to show better catalysis activity for OER.

Through the previous studies, it is known that the non-noble transition metals and their alloys of the eighth group have good activity for oxygen evolution reactions under alkaline conditions. Figure 4(A) compares the OER electrochemical activities of three cobalt oxide samples with different morphologies by linear sweep voltammetric (LSV) polarization curves. In the rotating disk electrode system, the working electrode was continuously rotated at a speed of 1600 $r \cdot min^{-1}$ in a 1 $mol \cdot L^{-1}$ KOH solution to remove the oxygen bubbles generated.

According to the Nernst equation $E_{RHE} = E_{Hg/HgO} + 0.0591 \times pH + 0.098$, the measured anode potential vs. Hg/HgO can be converted into the one vs. the standard

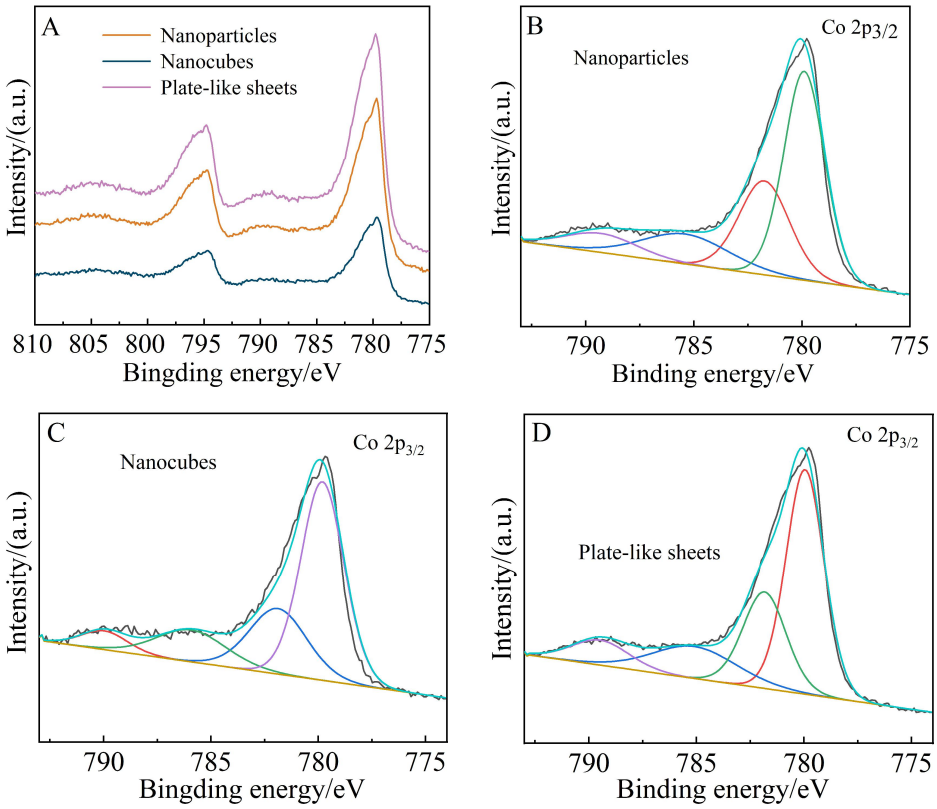

Figure 3. XPS spectra of Co_3O_4 particles with different morphologies (A); High-resolution XPS spectra of Co $2p_{3/2}$ for Nanoparticles (B); Nanocubes (C) and Plate-like sheets (D). (color on line)

Table 1. Fitting parameters for the Co $2p_{2/3}$ XPS spectra of Co_3O_4

Sample	Co^{3+} 779.8 eV	Co^{2+} 781.7 eV	Area ratio of Co^{3+}/Co^{2+}
Nanoparticles	472324	261451	1.81
Nanocubes	202091	88356	2.29
Plate-like sheets	464940	224563	2.07

hydrogen electrode (RHE). Therefore, the thermodynamic potential of electrodes is 1.23 V. The electrode potentials measured with the different types of cobalt oxide samples are compared when the current density is taken as 5 mA·cm^{-2}, and the specific values are shown in Table 2[26]. As depicted in Figure 4(A), the anode current of Plate-like sheets rised rapidly as it scanned toward the positive potential, and it required the smallest onset potential toward OER of 1.69 V where the activity began and afforded a current density of 5 mA·cm^{-2} at an overpotential of 460 mV. The apparently higher OER activity might be from the more active sites available on Plate-like sheets. Apart from OER activity, the stability is another critical parameter for evaluating the catalysts. We recorded the amperometric *i-t* curves for the three samples under 1.73 V vs. RHE in 1 mol·L^{-1} KOH electrolyte (Figure 4(B)). The results show that the current densities of the three samples were slightly higher than the values tested by LSV, but without significant changes during the 7200-s tests, indicating that the Co_3O_4 catalysts with different morphologies had better alkaline tolerance.

In order to compare the intrinsic activities of different crystal planes, the electrochemical double-layer capacitance is used to estimate and normalize the electrochemical catalytic surface area (ECSA) of each catalyst sample. Here, the cyclic voltammetry is used to test the charge and discharge currents of the electric double layer of the metal oxide within the potential range where no electrochemical reaction occurs[27]. In the linear relationship between the non-Faraday current of the metal oxide and the linear scan rate, the slope is the double-layer capacitance value of the sample. The electrochemical area is the ratio of the electric double layer capacitance of the electrode to the surface electric double layer of an ideal smooth oxide electrode. According to the related research, the surface electric double layer capacitance of an ideal smooth oxide is reported to be 60 μF·cm^{-2} [28]. Therefore, the specific values of electrochemical double layer capacitance, roughness factor and electrochemical catalytic surface area are shown in Table 3. It can be seen that the ECSA values of the three kinds of cobalt oxides are in the order of Nanocubes < Nanoparticles < Plate-like sheets. As depicted in Figure 4(G), the intrinsic activity of (100) facet was the highest in terms of ECSA normalized current density. This is also consistent with the literature: the higher the proportion of high-valence cobalt, the higher the intrinsic catalytic activity of the crystal face[29]. To further confirm the catalytic mechanism of three samples for OER, we plotted the Tafel slopes based on the ECSA normalized LSV curve. As shown in Figure 4(H), the Tafel slope of Nanocubes is calculated to be 56 mV·dec^{-1} and lower than those of the other two samples, which indicates that Nanocubes sample is a more efficient OER electrocatalyst.

Infrared (IR) spectroscopy is a very powerful experimental technique to study *in situ* electrocatalytic reactions on metal surfaces. Here, we carried out *in-situ* FT-IR experiment to detect adsorbed oxygenated species and OOH* intermediate in the reaction process. As we can see from Figure 5, the recorded IR bands of Nanoparticles, Nanocubes and Plate-like sheets took place around 1235, 1247 and 1239 cm^{-1}, and their intensities were gradually increased with the potential scanned from 1.23 to 1.83 V. The IR bands of three samples around 1235 ~ 1247 cm^{-1} could be attributed to the characteristic vibration adsorption of the surface-adsorbed superoxide (OOH_{ad})[30], which suggests that the OER process is dominated by the absorbed oxygen evolution mechanism over three kinds of cobalt oxides.

In order to further understand the structure-activity relationship of the cobalt oxide catalyst in the OER process and to reveal the active sites of the catalyst in the reaction process, the density functional theory (DFT) calculations on three facets of cobalt oxide catalysts were performed to rationalize the observed activity. On the (100) crystal plane, OH species are stably adsorbed on the Co site, where the Co-O bond length is 1.89 angstroms, and then, free OH attacks the adsorbed OH* species, and a molecule of H_2O desorbs to form adsorbed O* species, where the Co-O bond length is 1.95 angstroms, and OH^- contin-

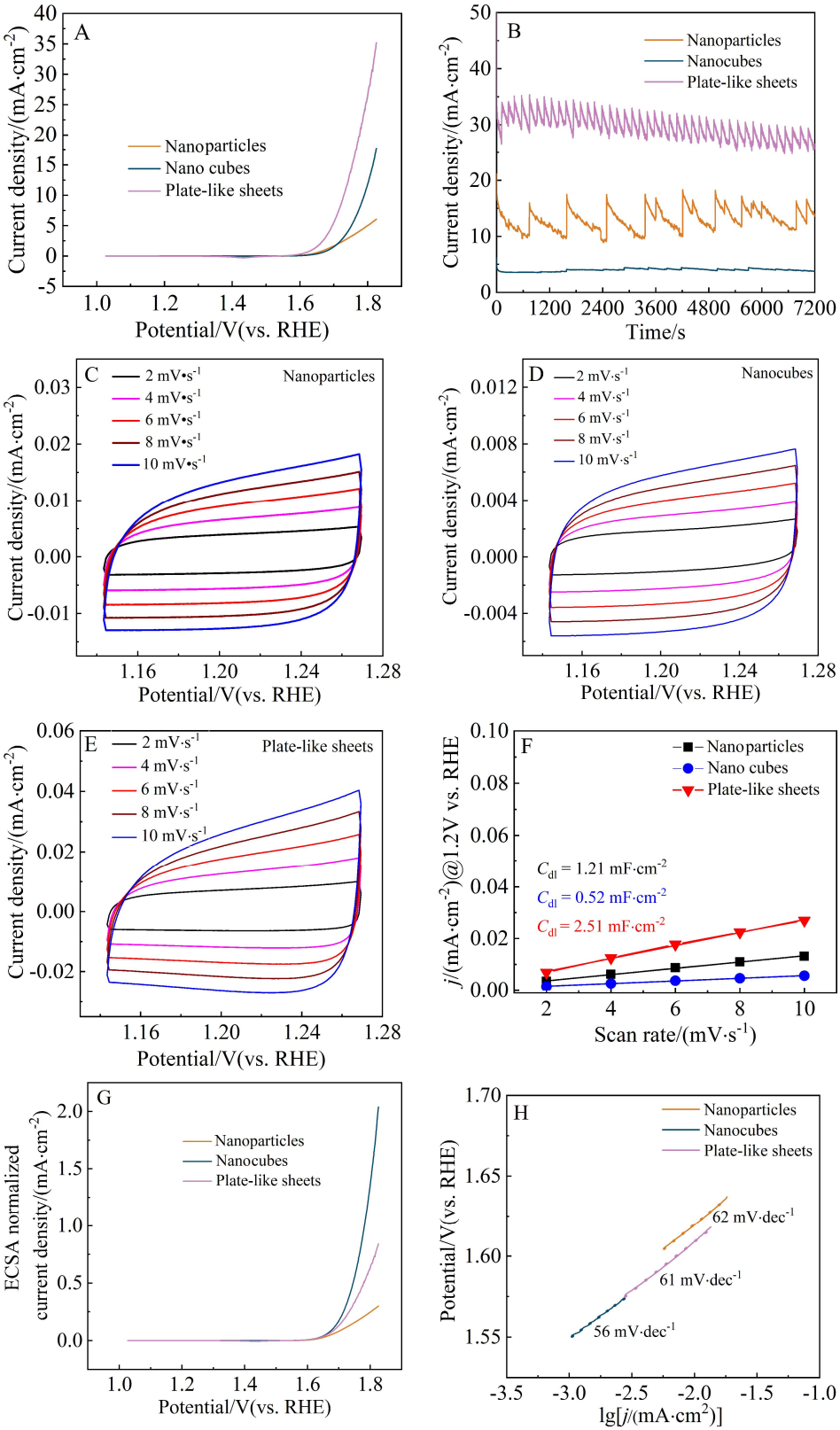

Figure 4. Electrochemical activity test of cobalt oxides with different shapes. (A) 5 mV·s^{-1} sweep rate LSV curves in 1 mol·L^{-1} KOH solution of Co_3O_4 nanoparticles with different morphologies; (B) Amperometric *i-t* curves of three samples during 7200-s test. (C) Cyclic voltammograms (CVs) of Nano particles; (D) Cyclic voltammograms (CVs) of Nanocubes; (E) Cyclic voltammograms (CVs) of Plate-like sheets measured at different scan rates from 2 to 10 mV·s^{-1}; (F) $\Delta J(=J_a - J_c)$ plotted against scan rates; (G) ECSA normalized LSV curves; (H) Tafel slopes of OER plotted based on the ECSA normalized LSV curves. (color on line)

Table 2. The electrode potentials of different Co_3O_4 samples at a current density of 5 mA·cm^{-2}

Sample	Nanoparticles	Nanocubes	Plate-like sheets
Electrode potential	1.80 V	1.75 V	1.69 V
Overpotential	570 mV	520 mV	460 mV

Table 3. Comparison of C_{dl} and R_f values for cobalt oxides

Sample	C_{dl}(mF·cm^{-2})	ECSA (cm^2)	R_f
Nanoparticles	1.21	2.42	20.17
Nanocubes	0.52	1.04	8.67
Plate-like sheets	2.51	5.02	41.83

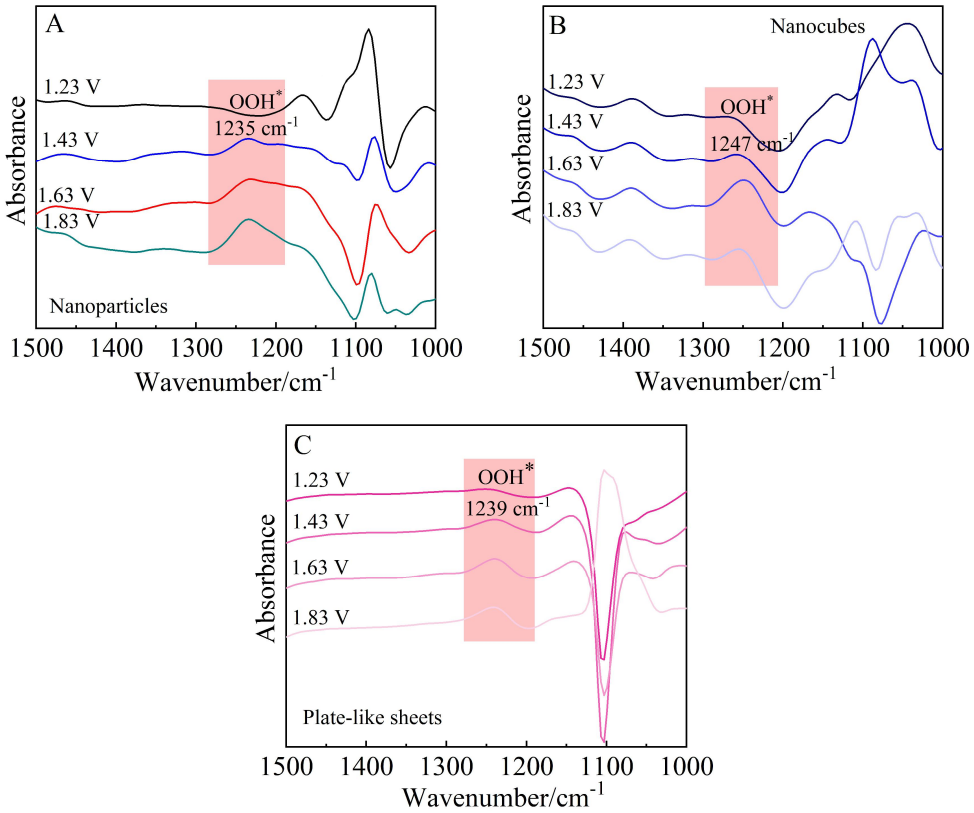

Figure 5. *In-situ* FT-IR spectra recorded at different potentials of cobalt oxides with various shapes. (A) Nanoparticles; (B) Nanocubes; (C) Plate-like sheets. Experiment conditions: Pt wire and Hg/HgO were used as the counter electrode and reference electrode, respectively, and electrolyte was 1 mol·L^{-1} KOH solution. FT-IR spectra were recorded after 60-s electrolysis at different potentials vs. RHE. (color on line)

ues to attack the O* species to form OOH*. OH^- continues to react with OOH* species to form a molecule of water and desorption of O_2. On the (110) crystal plane, OH species are stably adsorbed on the Co site, where the Co-O bond length is 1.616 angstroms, and then, free OH attacks the adsorbed OH* species, and a molecule of H_2O desorbs to form adsorbed O* species, where the Co-O bond length is 1.95 angstroms, and OH^- continues to attack the O* species to form OOH*. OH^- continues to react with OOH* species to

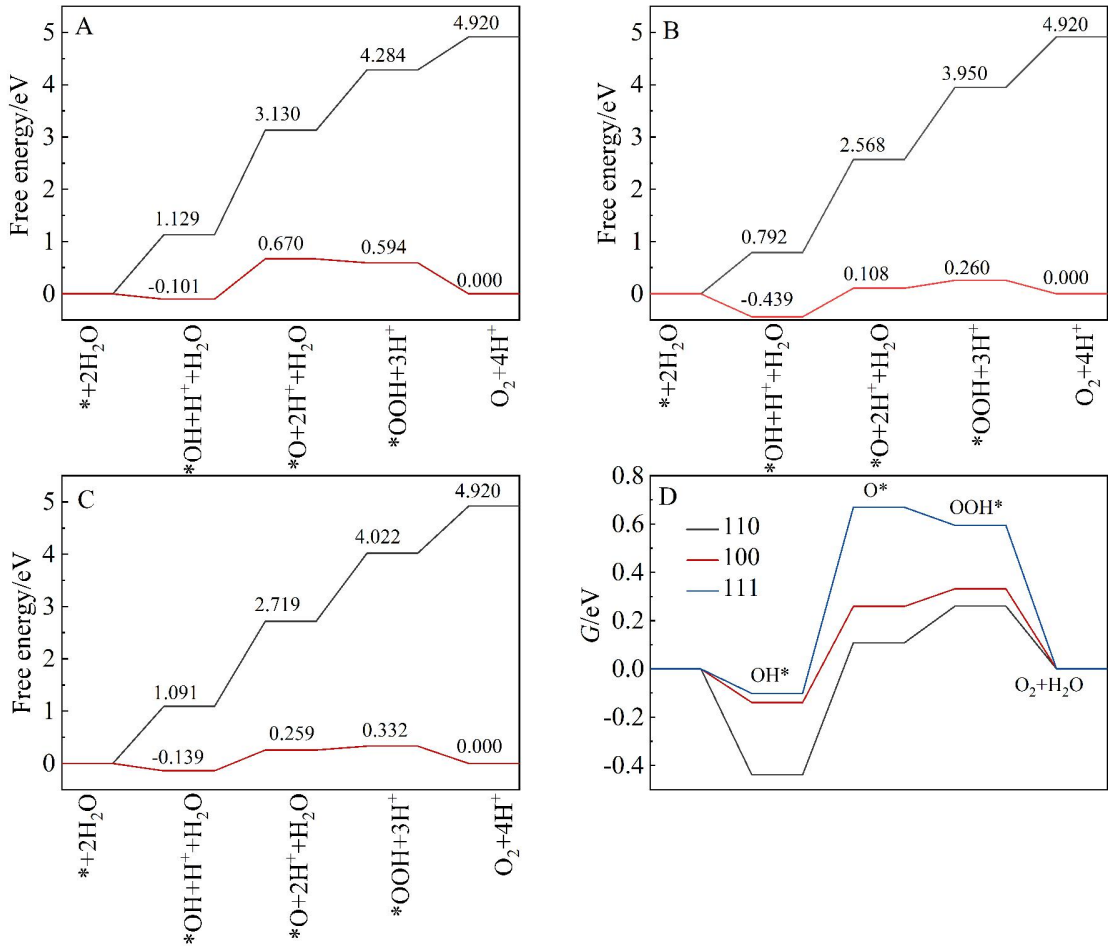

Figure 6. Energy diagrams of DFT calculations. Schematic energy profiles for the three typical (oxy)hydroxides on cobalt oxides in OER. (A) (111) crystal plane. (B) (100) crystal plane. (C) (110) crystal plane. The energy profiles presented here adopt the definition under an applied potential E = 0 V versus RHE (the black line) and an applied potential E = 1.23 V versus RHE (the red line). D: Comparison in different crystal planes of cobalt oxides under an applied potential E = 1.23 V versus RHE. (color on line)

form a molecule of water and desorption of O_2. On the (111) crystal plane, OH species are stably adsorbed on the Co site, where the Co-O bond length is 1.781 angstroms, and then, free OH attacks the adsorbed OH* species, and a molecule of H_2O desorbs to form adsorbed O* species, where the Co-O bond length is 1.628 angstroms, and OH^- continues to attack the O* species to form OOH*. OH^- continues to react with OOH* species to form a molecule of water and desorption of O_2. Compare and analyze the results at the equilibrium potential U = 1.23 V on the three crystal planes, as shown in Figure 6. By calculations, it can be obtained that the over potential (η) values of (111), (100) and (110) crystal planes are 0.77 V, 0.40 V, and 0.55 V, respectively, that is, $\eta_{100} < \eta_{110} < \eta_{111}$, which is consistent with the above experimental results.

4 Conclusions

Spinel cobalt oxides with three different morphologies, including nanoparticles, nanocubes, and nanoplates, have been synthetized using a facile hydrothermal method. Among them, the nanocubes with the exposed (100) facet offered the best intrinsic activity for oxygen evolution reaction (OER), which could be attributed to the most available Co^{3+} active sites on the nanocubes surface detected by XPS. DFT calculations also proved that the lowest energy barrier is achieved for oxygen evolution at the (100) facet. This study shows that the regulation of crystal plane is an important factor to design highly efficient OER catalysts.

Acknowledgements:

The authors are grateful for the financial supports from the Science and Technology Major Project of Tianjin (Grant Nos. 19ZXNCGX00030 and 20JCYBJC00870), and the National Nature Science Foundation of China (Grant Nos. 21938008 and 22078232).

References:

[1] Jamesh M I, Sun X M. Recent progress on earth abundant electrocatalysts for oxygen evolution reaction (OER) in alkaline medium to achieve efficient water splitting - A review[J]. J. Power Sources, 2018, 400: 31-68.

[2] Jiang H, Gu J X, Zheng X S, Liu M, Qiu X Q, Wang L B, Li W Z, Chen Z F, Ji X B, Li J. Defect-rich and ultrathin N doped carbon nanosheets as advanced trifunctional metal-free electrocatalysts for the ORR, OER and HER[J]. Energy Environ. Sci., 2019, 12(1): 322-333.

[3] Jahan M, Liu Z L, Loh K P. A Graphene oxide and copper-centered metal organic framework composite as a tri-functional catalyst for HER, OER, and ORR[J]. Adv. Funct. Mater., 2013, 23(43): 5363-5372.

[4] Zhang L H, Fan Q, Li K, Zhang S, Ma X B. First-row transition metal oxide oxygen evolution electrocatalysts: regulation strategies and mechanistic understandings[J]. Sustain. Energy Fuels, 2020, 4(11): 5417-5432.

[5] Jamesh M I, Harb M. Tuning the electronic structure of the earth-abundant electrocatalysts for oxygen evolution reaction (OER) to achieve efficient alkaline water splitting - A review[J]. J. Energy Chem., 2021, 56: 299-342.

[6] Zhang S, Fan Q, Xia R, Meyer T J. CO_2 reduction: from homogeneous to heterogeneous electrocatalysis[J]. Accounts Chem. Res., 2020, 53(1): 255-264.

[7] Liu H, Su Y Q, Kuang S Y, Hensen E J M, Zhang S, Ma X B. Highly efficient CO_2 electrolysis within a wide operation window using octahedral tin oxide single crystals[J]. J. Mater. Chem. A, 2021, 9(12): 7848-7856.

[8] Karmakar A, Karthick K, Sankar S S, Kumaravel S, Madhu R, Kundu S. A vast exploration of improvising synthetic strategies for enhancing the OER kinetics of LDH structures: a review[J]. J. Mater. Chem. A, 2021, 9(3): 1314-1352.

[9] Duan Y, Sun S N, Sun Y M, Xi S B, Chi X, Zhang Q H, Ren X, Wang J X, Ong S J H, Du Y H, Gu L, Grimaud A, Xu Z C J. Mastering surface reconstruction of metastable spinel oxides for better water oxidation[J]. Adv. Mater., 2019, 31(12): 1807898.

[10] Sun Y M, Liao H B, Wang J R, Chen B, Sun S N, Ong S J H, Xi S B, Diao C Z, Du Y H, Wang J O, Breese M B H, Li S Z, Zhang H, Xu Z C J. Author Correction: Covalency competition dominates the water oxidation structure-activity relationship on spinel oxides[J]. Nat. Catal., 2020, 3(11): 959.

[11] Reier T, Oezaslan M, Strasser P. Electrocatalytic oxygen evolution reaction (OER) on Ru, Ir, and Pt Catalysts: A comparative study of nanoparticles and bulk materials[J]. ACS Catal., 2012, 2(8): 1765-1772.

[12] Acedera R A E, Gupta G, Mamlouk M, Balela M D L. Solution combustion synthesis of porous Co_3O_4 nanoparticles as oxygen evolution reaction (OER) electrocatalysts in alkaline medium[J]. J. Alloy. Compd., 2020, 836: 154919.

[13] Wang C X, Shi P H, Cai X D, Xu Q J, Zhou X J, Zhou X L, Yang D, Fan J C, Min Y L, Ge H H, Yao W F. Synergistic effect of Co_3O_4 nanoparticles and graphene as catalysts for peroxymonosulfate-based orange II degradation with high oxidant utilization efficiency[J]. J. Phys. Chem. C, 2016, 120(1): 336-344.

[14] Xiao Z, Huang Y C, Dong C L, Xie C, Liu Z J, Du S Q, Chen W, Yan D F, Tao L, Shu Z W, Zhang G H, Duan H G, Wang Y Y, Zou Y Q, Chen R, Wang S Y. Operando identification of the dynamic behavior of oxygen vacancy-rich Co_3O_4 for oxygen evolution reaction[J]. J. Am. Chem. Soc., 2020, 142(28): 12087-12095.

[15] Peng Y, Hajiyani H, Pentcheva R. Influence of Fe and Ni Doping on the OER Performance at the Co_3O_4 (001) Surface: Insights from DFT+ U Calculations[J]. ACS Catal., 2021, 11(9): 5601-5613.

[16] Xu L, Jiang Q Q, Xiao Z H, Li X Y, Huo J, Wang S Y, Dai L M. Plasma-engraved Co_3O_4 nanosheets with oxygen vacancies and high surface area for the oxygen evolution reaction[J]. Angew. Chem. Int. Ed., 2016, 128(17): 5363-5367.

[17] Zhang Y X, Ding F, Deng C, Zhen S Y, Li X Y, Xue Y F, Yan Y M, Sun K N. Crystal plane-dependent electrocatalytic activity of Co_3O_4 toward oxygen evolution reaction[J]. Catal. Commun., 2015, 67: 78-82.

[18] Liu L, Jiang Z Q, Fang L, Xu H T, Zhang H J, Gu X, Wang Y. Probing the crystal plane effect of Co_3O_4 for enhanced electrocatalytic performance toward efficient overall water splitting[J]. ACS Appl. Mater. Inter., 2017, 9(33): 27736-27744.

[19] Liu Q F, Chen Z P, Yan Z, Wang Y, Wang E D, Wang S, Wang S D, Sun G Q. Crystal-plane-dependent activity of spinel Co_3O_4 towards water splitting and the oxygen reduction reaction[J]. ChemElectroChem, 2018, 5(7): 1080-

1086.

[20] Zhu K Y, Zhu X F, Yang W S. Application of *in situ* techniques for the characterization of NiFe-based oxygen evolution reaction (OER) electrocatalysts[J]. Angew. Chem. Int. Ed., 2019, 58(5): 1252-1265.

[21] Xiao X L, Liu X F, Zhao H, Chen D F, Liu F Z, Xiang J H, Hu Z B, Li Y D. Facile shape control of Co_3O_4 and the effect of the crystal plane on electrochemical performance[J]. Adv. Mater., 2012, 24(42): 5762-5766.

[22] Zhang J J, Wang H H, Zhao T J, Zhang K X, Wei X, Li X H, Hirano S I, Chen J S. Oxygen vacancy engineering of Co_3O_4 nanocrystals through coupling with metal support for water oxidation[J]. ChemSusChem, 2017, 10(14): 2875-2879.

[23] He D, Song X Y, Li W Q, Tang C Y, Liu J C, Ke Z J, Jiang C Z, Xiao X H. Active electron density modulation of Co_3O_4-based catalysts enhances their oxygen evolution performance[J]. Angew. Chem. In.t Ed., 2020, 132(17): 6996-7002.

[24] Kumar K, Canaff C, Rousseau J, Arrii-Clacens S, Napporn T W, Habrioux A, Kokoh K B. Effect of the oxide-carbon heterointerface on the activity of Co_3O_4/NRGO nanocomposites toward ORR and OER[J]. J. Phys. Chem. C, 2016, 120(15): 7949-7958.

[25] Tang D, Ma Y, Liu Y, Wang K K, Liu Z, Li W Z, Li J. Amorphous three-dimensional porous Co_3O_4 nanowire network toward superior OER catalysis by lithium-induced[J]. J. Alloy Compd., 2021, 893: 162287.

[26] Zhou X M, Xia Z M, Tian Z M, Ma Y Y, Qu Y Q. Ultrathin porous Co_3O_4 nanoplates as highly efficient oxygen evolution catalysts[J]. J. Mater. Chem. A, 2015, 3(15): 8107-8114.

[27] McCrory C C L, Jung S, Peters J C, Jaramillo T F. Benchmarking heterogeneous electrocatalysts for the oxygen evolution reaction[J]. J. Am. Chem. Soc., 2013, 135(45): 16977-16987.

[28] Ma T Y, Dai S, Jaroniec M, Qiao S Z. Metal-organic framework derived hybrid Co_3O_4-carbon porous nanowire arrays as reversible oxygen evolution electrodes[J]. J. Am. Chem. Soc., 2014, 136(39): 13925-13931.

[29] Song K, Cho E, Kang Y M. Morphology and active-site engineering for stable round-trip efficiency Li-O_2 batteries: A search for the most active catalytic site in Co_3O_4[J]. ACS Catal., 2015, 5(9): 5116-5122.

[30] Yao Y C, Hu S L, Chen W X, Huang Z Q, Wei W C, Yao T, Liu R R, Zang K T, Wang X Q, Wu G, Yuan W J, Yuan T W, Zhu B Q, Liu W, Li Z J, He D S, Xue Z G, Wang Y, Zheng X S, Dong J C, Chang C R, Chen Y X, Hong X, Luo J, Wei S Q, Li W X, Strasser P, Wu Y E, Li Y D. Engineering the electronic structure of single atom Ru sites via compressive strain boosts acidic water oxidation electrocatalysis[J]. Nat. Catal., 2019, 2(4): 304-313.

尖晶石钴氧化物的晶面调控与析氧活性研究

张丽桦[1,2],揣宏媛[1*],刘 海[1],范 群[1],况思宇[1],张 生[1,3*],马新宾[1,3]

(1. 天津大学化工学院,绿色化工技术教育部重点实验室,天津 300072;
2. 中国石油天然气股份有限公司,兰州化工研究中心,化工催化剂研究所,甘肃 兰州 730060;
3. 天津大学浙江研究院,浙江 宁波 345201)

摘要: 由可再生能源驱动的水分解是一种有前途的生产清洁能源的技术,而发生在阳极的析氧反应是水分解反应的速率决定步骤。本文通过调整催化剂的晶面,暴露更多的有效活性位点调控尖晶石钴氧化物析氧反应活性。在三个合成晶面(100)、(111)和(110)中,(100)晶面本征活性最高。结合原位红外和 DFT 计算分析可知,OER 反应在氧化钴晶体的(100)平面上反应能垒最低。XPS 分析进一步表明,纳米立方体表面具有最高的 Co^{3+}/Co^{2+} 比值,该结果表明 Co^{3+} 是更活跃的析氧反应活性位点。

关键词: 电解水;析氧反应;尖晶石钴氧化物;晶面依赖性;纳米立方体